

Using reinforcement learning to probe the role of feedback in skill acquisition

Antonio Terpin*
ETH Zürich
aterpin@ethz.ch

Raffaello D'Andrea
ETH Zürich
rdandrea@ethz.ch

Abstract

Many high-performance human activities are executed with little or no external feedback: think of a figure skater landing a triple jump, a pitcher throwing a curveball for a strike, or a barista pouring latte art. To study the process of skill acquisition under fully controlled conditions, we bypass human subjects. Instead, we directly interface a generalist reinforcement learning agent with a spinning cylinder in a tabletop circulating water channel to maximize or minimize drag. This setup has several desirable properties. First, it is a physical system, with the rich interactions and complex dynamics that only the physical world has: the flow is highly chaotic and extremely difficult, if not impossible, to model or simulate accurately. Second, the objective—drag minimization or maximization—is easy to state and can be captured directly in the reward, yet good strategies are not obvious beforehand. Third, decades-old experimental studies provide recipes for simple, high-performance open-loop policies. Finally, the setup is inexpensive and far easier to reproduce than human studies. In our experiments we find that high-dimensional flow feedback lets the agent discover high-performance drag-control strategies with only minutes of real-world interaction. When we later replay the same action sequences without any feedback, we obtain almost identical performance. This shows that feedback, and in particular flow feedback, is not needed to execute the learned policy. Surprisingly, without flow feedback during training the agent fails to discover any well-performing policy in drag maximization, but still succeeds in drag minimization, albeit more slowly and less reliably. Our studies show that learning a high-performance skill can require richer information than executing it, and learning conditions can be kind or wicked depending solely on the goal, not on dynamics or policy complexity.

<https://antonioterpin.com/fluids-control>

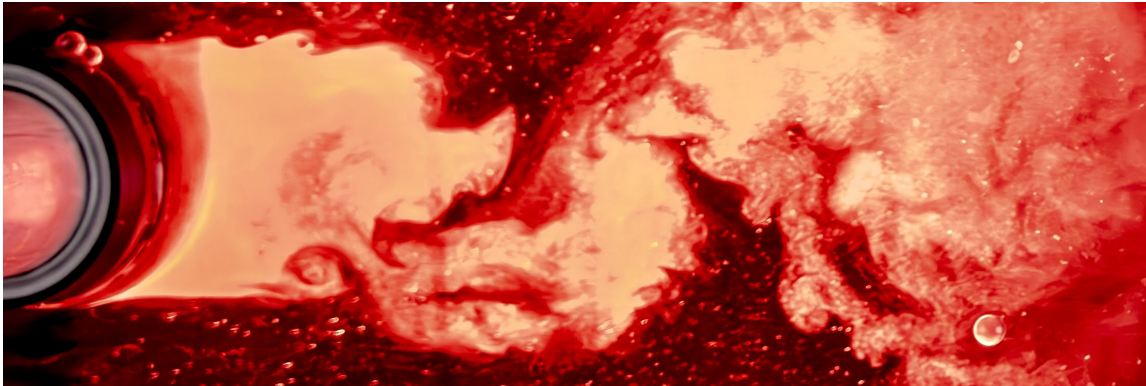


Figure 1: Wake behind the cylindrical body considered in this study.

*Corresponding author.

Contents

1 Our findings	1
2 Learning to control fluids	4
3 Results	4
3.1 The reinforcement learning (RL) agent rapidly masters the tasks when provided with flow feedback, but fails to find high-performance drag-maximizing policies without	5
3.2 The learned strategies can be performed in open-loop	6
3.3 Early measurements anti-align with long-run performance	8
4 Discussion	8
4.1 Privileged information and observation-adaptive agents	8
4.2 Quantifying the value of feedback for learning	9
5 Conclusion	10
References	11
A A tabletop circulating water channel (CWC)	17
B Related work in fluids control	18
C The performance of open-loop control	20
D Additional information on the data acquisition pipeline	20
D.1 Additional sources of uncertainty	21
D.2 Additional experiment to verify that the cylinder dynamics are inconsequential for the torque sensor measurements	21
D.3 Additional details on the vision pipeline	21
E Ablations	22
E.1 Ablations on the observation sets	22
E.2 Ablations on the model size	23
E.3 Ablations on how to remove the flow feedback	23
E.4 Ablations on the learning algorithm	24

1 Our findings

Humans often rely heavily on feedback during the acquisition of new skills, yet once a skill is mastered, it can often be executed with minimal or no reliance on that feedback. This phenomenon is observed especially in motor skills. For example, as demonstrated by [Lee and Aronson \[1974\]](#) and [Anderson et al. \[2019\]](#), a toddler learning to walk uses visual and proprioceptive feedback to adjust each step, whereas an adult walks effortlessly (almost “open-loop”) without consciously monitoring each foot placement. Similarly, athletes like figure skaters, gymnasts and dancers receive constant feedback (from coaches, mirrors, etc.) in training, but during performance they rely on internalized “motor programs” rather than external feedback. The shift from feedback (closed-loop) control in novice performance to open-loop control in expert performance is central to classical motor learning theories, such as the ones presented by [Adams \[1971\]](#) and [Schmidt \[1975\]](#). In the words of [Malone et al. \[2025\]](#), “the control of movement gradually transitions from feedback control to feedforward adaptation”, and the learner becomes less reliant on feedback with practice.

To relate to the scope of our work, consider the following game. First, you crumple a scrap of paper into a ball and throw it a few meters away. You look carefully to note where it lands, then close your eyes and walk toward where you think it is, trying to pick it up without peeking.



When you reach down, you will often find you are just a little off. Now, suppose you are allowed to peek only once. You will likely be able to succeed all the time. This playful experiment prompts two observations. First, without any visual feedback we are capable of getting fairly close to the objective. Second, with a minimal amount of visual feedback we are certain to complete the task. These observations suggest that many of the skills exploited in this task require less feedback than what we have available. In fact, walking is certainly an activity that is possible to perform without any feedback (albeit perhaps with lower “accuracy”), as shown with a machine by [McGeer et al. \[1990\]](#) and empirically in humans by [Souman et al. \[2009\]](#), [Iosa et al. \[2012\]](#), [Naaman et al. \[2023\]](#). But could we *learn* to walk without any feedback? The experimental results of [Lee and Aronson \[1974\]](#) and [Anderson et al. \[2019\]](#) seem to suggest that visual feedback, at least, is used by infants. On the other hand, the studies by [Kasuga et al. \[2015\]](#), [Raichin et al. \[2021\]](#) seem to suggest that when one is interested in improving the open-loop component of a policy, providing feedback is detrimental. This result is somewhat intuitive, but there is a subtle catch: since the human participants are adults, their motor control is not a “clean slate”, as the participants carry a whole set of motor skills that can be exploited when learning a new task.

These studies, together with our everyday experience, motivate asking how feedback shapes skill acquisition. However, answering this question directly with human participants is difficult. Systematic ablations of sensory feedback are ethically and practically constrained: one cannot easily and fully control exteroceptive and proprioceptive feedback. Constructing appropriate control groups is also challenging, since human learners arrive with a lifetime of prior experience that any new task inevitably leverages in ways that are hard to quantify or standardize. Finally, carefully controlled motor-learning experiments are time-consuming and expensive, making systematic ablations over feedback modalities prohibitive. In this work, we take a complementary approach: we keep human motor learning as our guiding analogy, but we do not experiment with people. Instead, we use the generalist, state-of-the-art RL algorithm DreamerV3 from [Hafner et al. \[2025\]](#), without any hyperparameter tuning or inductive bias, as a scientific instrument to dissect the role of feedback in the acquisition of open-loop skills, enabling clean and causal interventions. The extensive numerical evidence collected in this project would be practically unattainable

in human-subject experiments, given the prohibitive logistical and financial costs.

Previous work proved DreamerV3 capable of learning to play Minecraft [Hafner et al., 2025], perform tactile insertion [Palenicek et al., 2024], play a real-world labyrinth game [Bi and D’Andrea, 2024], control a quadrotor [Romero et al., 2025]. Unlike Ma et al. [2023], Abdi et al. [2020], Srungarapu [2021], Garibbo et al. [2022], we do not impose a structural bias toward open-loop policies or use a brain-inspired architecture [Baladron et al., 2023]; instead, we study how open-loop policies *emerge*. For this, we interface the DreamerV3 RL algorithm by Hafner et al. [2025] with the tabletop circulating water channel (CWC) depicted in Figure 2 and detailed in Section A to learn to minimize and maximize the drag experienced by a spinning cylinder immersed in a fluid flow.

We consider this system because it satisfies several desirable properties. First, it is a physical system, with the rich interactions and complex dynamics that only the physical world has: it is an infinite-dimensional nonlinear system governed by the Navier–Stokes equations. At the Reynolds numbers and blockage factor of interest, the wake is strongly chaotic and highly sensitive to small geometric and surface-condition details, so high-fidelity simulations generally require substantial computational resources, aggressive simplifications, and still suffer from a significant sim-to-real gap; see Section B. Second, the control objective—drag minimization or maximization—is simple and can be specified via a dense reward, yet the complexity of the dynamics makes effective strategies non-obvious. Third, classic flow-control studies [Coutanceau and Menard, 1985, Badr and Dennis, 1985] show that simple open-loop laws can nonetheless achieve high performance. Finally, the tabletop platform is low-cost, and we release the hardware designs and software implementation, making the experiments straightforward to reproduce and extend in other laboratories, unlike typical human studies.

Contributions. We use a generalist RL agent as a scientific instrument to probe how feedback shapes the difficulty of learning control in a real, chaotic fluid system. We find that:

- (i) A generalist agent—without inductive biases or hyperparameter tuning—trained with dense flow feedback on the setup in one-minute episodes (1800 steps) finds a high-performance strategy in a few minutes. In contrast, the latest result in RL for fluids control [Ye and Elsheikh, 2025] (without dense flow feedback and in a two-dimensional simulation) requires several hours (~ 10) for two-second episodes (80 steps). To our knowledge, this is the first demonstration of RL for fluids control with dense flow feedback on hardware and rapid training (see Section B), showing that agents can be trained directly from interaction with the underlying flow rather than from tuned simulations that inevitably reflect modeling assumptions.
- (ii) Rollout trajectories define open-loop strategies: replaying them without any feedback nearly matches online performance, with only a slight edge in drag maximization. As in our crumpled paper game, feedback only supplies a “last mile” correction.
- (iii) Contrasting drag minimization and maximization shows that the same physical system presents kind or wicked learning conditions depending solely on the goal, not on the dynamics and policy complexity. In drag minimization, the agent discovers well-performing strategies even without flow feedback. In drag maximization, training without flow feedback consistently fails: early measurements are anti-correlated with long-run performance, an effect we connect to dynamical-systems theory and non-minimum-phase behavior [Åström and Murray, 2021]. This suggests that, in complex physical systems, the information needed to *learn* a high-performance policy can be substantially richer than the information needed to *execute* it.

We conclude by discussing these findings and motivating architectures that exploit rich feedback during learning but selectively ignore it at execution, except to recover the last mile of performance.

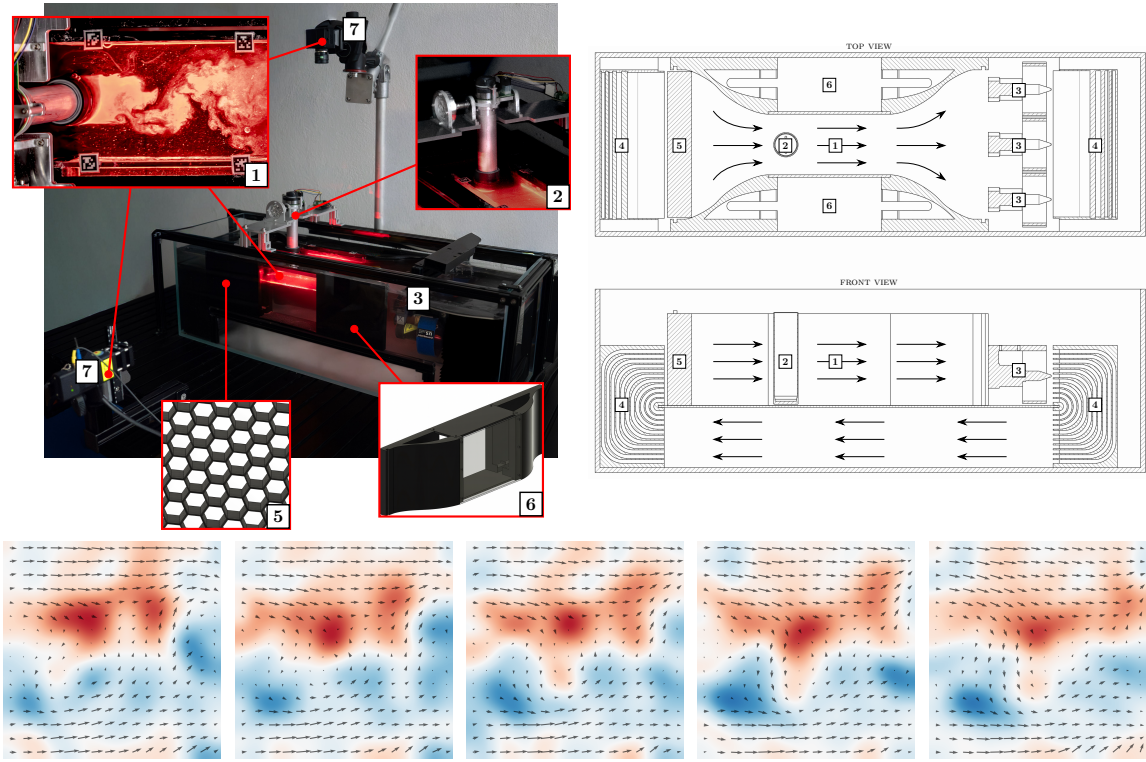
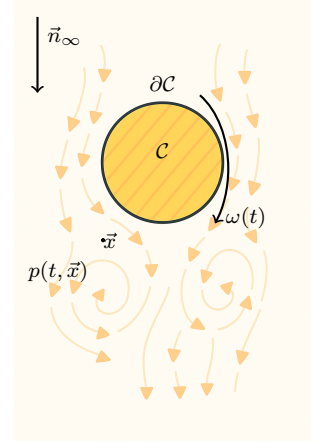


Figure 2: Top: Our tabletop CWC with close-ups of the main components and its top and side view. The channel consists of an upper and a lower branch. The test section (1) in the upper branch houses the cylinder (2). Three APISQUEEN U5 brushless freshwater propellers (3) drive a left-to-right flow, which is redirected into the lower branch by guide vanes (4) and then back to the upper branch. A honeycomb structure (5) straightens the flow and suppresses large-scale vortices. Flow restrictions (6) accelerate the stream and stretch remaining small-scale vortices. Below: Illustrative snapshots of the real-time flow estimates from the imaging setup (7); colors indicate vorticity (red/blue: positive/negative).

2 Learning to control fluids

As early as the 1980s, Coutanceau and Menard [1985], Badr and Dennis [1985] (among others) observed that vortex shedding behind a circular cylinder \mathcal{C} of radius R in a uniform flow can be reduced or even suppressed by spinning the cylinder at a (possibly time-dependent) angular velocity $\omega(t)$. The resulting unsteady surface pressure $p(t, \vec{x})$ on $\partial\mathcal{C}$ is governed by the incompressible Navier–Stokes equations for a Newtonian fluid of density ρ and kinematic viscosity ν (e.g., Acheson, 1990), $\partial_t \vec{u} + (\vec{u} \cdot \nabla) \vec{u} = -\frac{1}{\rho} \nabla p + \nu \nabla^2 \vec{u}$, $\nabla \cdot \vec{u} = 0$, subject to appropriate boundary conditions (e.g., incoming flow stream, no-slip at the walls). Commanding a rotation rate $\omega(t)$ imposes $\vec{u}(t, \vec{x}) = R\omega(t)\vec{t}_{\mathcal{C}}(\vec{x})$ for all $\vec{x} \in \partial\mathcal{C}$, with $\vec{t}_{\mathcal{C}}(\vec{x})$ being the vector tangent to \mathcal{C} at \vec{x} . As a result, controlling the rotation rate $\omega(t)$ of the cylinder alters the pressure and, thus, the resulting force (drag) on the cylinder, which can then be taken as a performance metric to either minimize or maximize. Despite the complexity of the system dynamics, a high-performance strategy is open-loop: $\omega(t) = A \sin(2\pi ft)$ for some A, f .



Accurately simulating such a fluid setup is challenging: even idealized 2D models with ideal boundary conditions are prohibitively slow and often fail to capture essential physical properties; realistic 3D simulations with active control are even more intractable, making systematic studies and ablations impractical. Because no open-source testbed for fluids control exists, we built a low-cost physical platform, shown in Figure 2 and detailed in Section A. Using modern accelerators, we compute dense flow estimates in real time and train an RL agent directly on the physical system with these as feedback. To our knowledge, this is the first such demonstration; see Section B.

Deploying RL to control fluids. For an overview of the system, see Figure 3. We use the DreamerV3 architecture with default hyperparameters and the standard model with 25 million parameters. The agent selects a one-dimensional continuous action in $[-\bar{A}, \bar{A}]$ commanding the cylinder’s instantaneous rotation rate, which we normalize to $[-1, 1]$ for learning. The agent observations consist of the drag measurement, the commanded rotation rate (the action), rotation-rate feedback from the motor and, optionally, a dense flow estimate (see Section D.3). We take these configurations as representative since one only has the reward signal, the commanded rotation rate (the previous action of the agent) and a proprioceptive feedback signal (the rotation-rate feedback) to work with, whereas the other has, additionally, the exteroceptive feedback (the flow field) on the system state. The decrease (drag-minimization task) or increase (drag-maximization task) of the drag measurement with respect to its value at the beginning of the episode is the reward signal, and we always provide the drag measurement as an observation to the agent. Episodes last 60 s, and in between episodes we wait 60 s to stabilize the flow. Training uses a 60-minute budget (60 episodes), corresponding to 100,800 environment steps.

3 Results

Next, we present the experimental results supporting Section 1. The *Baseline* is the average outcome of a high-performance sinusoidal input (Section C), and we normalize the results by the average no-control outcome across experiments; see Section A.

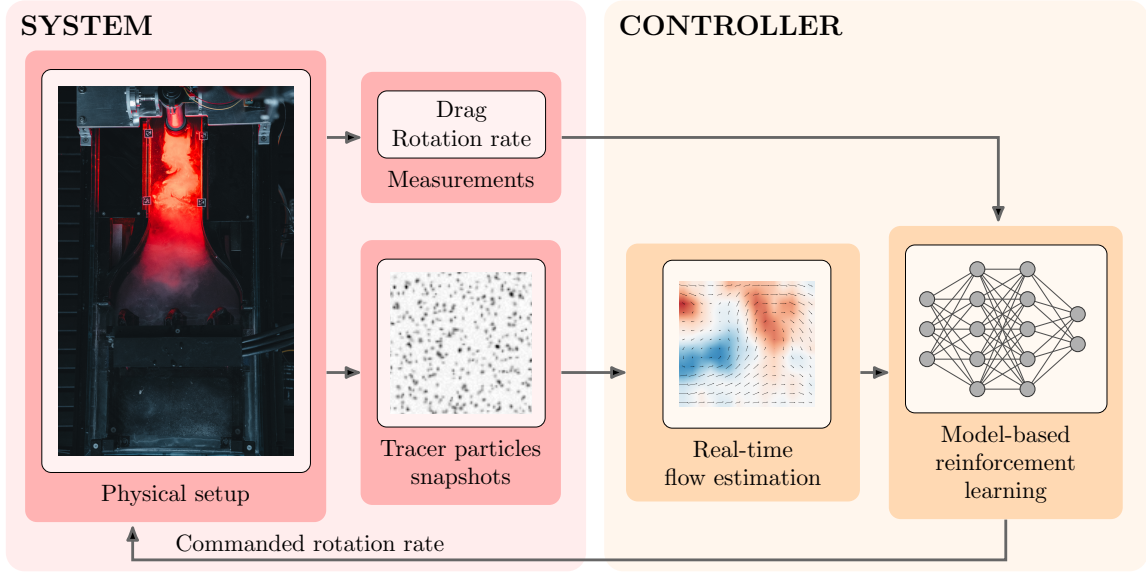


Figure 3: System overview. The RL agent interacts directly with the physical setup, commanding the rotation rate of the cylinder, receiving as observations the previous commanded rotation rate, the drag on the cylinder, the motor rotation-rate feedback, and possibly the flow estimate from the camera images of neutrally buoyant tracer particles. We compare learning performance under different observation sets.

3.1 The RL agent rapidly masters the tasks when provided with flow feedback, but fails to find high-performance drag-maximizing policies without

Experimental setup. We train agents with and without flow feedback and measure the change in drag relative to its value at the beginning of each episode (a decrease for drag minimization, an increase for drag maximization). We repeat each training run ten times. We perform several observation-set ablations in Section E.1.

Results. In Figure 4, we report training curves for models with and without flow feedback, which are consistent across repetitions.

In both tasks, the configuration with flow feedback rapidly and robustly (i.e., with low variability) discovers a high-performance policy within minutes of real-world interaction. Without flow feedback, the agent fails to find a high-performance policy in the drag-maximization task but still succeeds in drag minimization, albeit more slowly and with greater variability.

This is perhaps surprising: as we show in Section C, simple sinusoidal action sequences can be highly effective, so there exists a class of policies that performs well without flow feedback. Even though the tasks share the same physical system, admit high-performance policies of similar complexity, and differ in reward only by a sign, the lack of flow feedback during training has strongly asymmetric effects: the agent succeeds in drag minimization but fails in drag maximization. Thus, the same physical system presents kind or wicked learning conditions depending solely on the goal, not on dynamics or policy complexity. We investigate these conditions next.

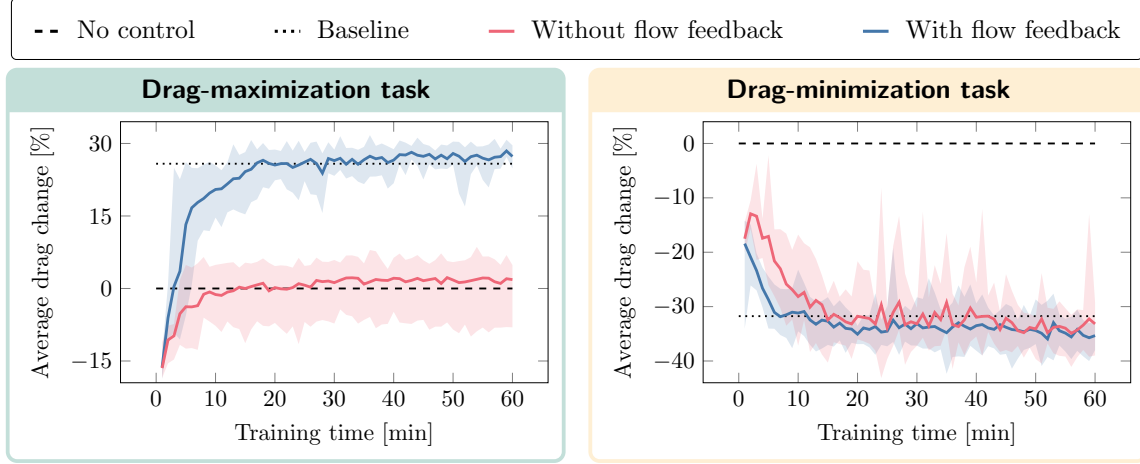


Figure 4: Running-average drag variation (%) with respect to no control) in the episode over training time (min) for DreamerV3 with and without flow feedback for the drag-maximization (left) and drag-minimization (right) tasks. The solid lines show the mean performance of the model across repetitions, whereas the shaded areas show min-max variability.

3.2 The learned strategies can be performed in open-loop

Experimental setup. We record the action trajectories all throughout the training process for the agent with all observations, including the flow estimate. Then, we replay these action trajectories without any feedback five times each and observe the resulting performance.

Results. We summarize the results in Figure 5. Replayed trials produce reward trajectories that closely track those obtained during online execution, indicating that the agent has learned a primarily open-loop strategy whose outcomes are stable across repeats. Even early in training, an action sequence rollout achieves similar performance when replayed, suggesting a turnpike-like property [Dorfman et al., 1987] and that good performance in this task does not primarily rely on real-time feedback, but on finding high-performing open-loop trajectories. In the drag-minimization task, feedback offers no measurable advantage: replayed trajectories match online performance within experimental variability. In the drag-maximization task, however, the absence of feedback yields a modest but consistent drop relative to online execution, suggesting that feedback is used mainly for small corrective adjustments on top of an essentially open-loop plan. This pattern mirrors the paper-ball game from Section 1: as a person can walk with eyes closed to roughly where the ball should be and use a quick glance for the last correction, our agent learns an internalized open-loop program with high performance, with feedback providing a last-mile correction rather than a continuous crutch at execution.

Together with Section 3.1, these results suggest that, perhaps surprisingly, flow feedback is needed to learn a drag-maximizing policy that can be executed in open loop with comparable performance. Thus, in a complex physical system the information required to learn a high-performance skill can be substantially richer than the information required to execute it.

To our knowledge, this is the first empirical demonstration in real turbulent flow of such phenomena.

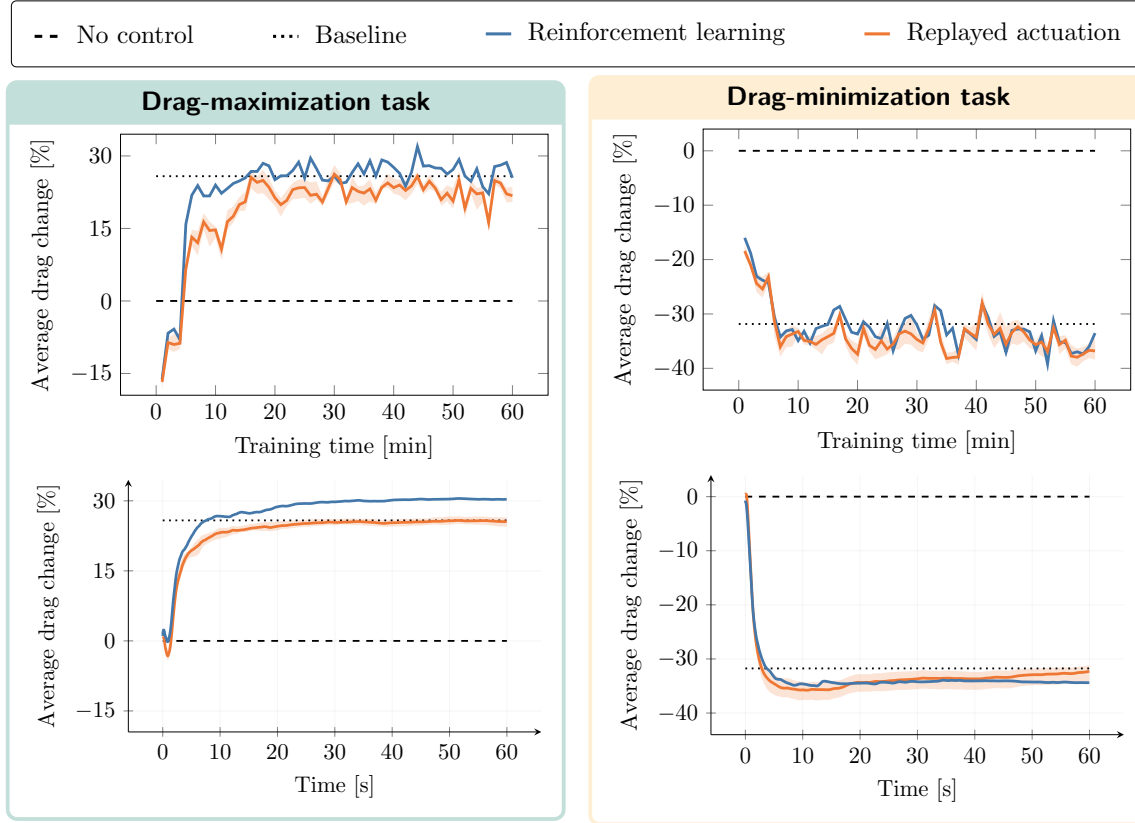


Figure 5: Running-average drag variation (%) with respect to no control) for the drag-maximization (left) and drag-minimization (right) tasks. Shown are the no-control mean (black dashed), best open-loop mean (gray dotted), RL (blue), and replayed actuation (red, mean over five repeats; shading shows min-max variability). Top: We show the curve over training time (minutes). Bottom: We show the curve for a single rollout, over episode time (seconds).

3.3 Early measurements anti-align with long-run performance

We can rule out several intuitive explanations for the observed behavior. The phenomenon is not an artifact of a particular choice of observations, as it persists across different observation sets; see Section E.1. In these sets, we also include a time signal, ruling out state aliasing [Whitehead and Ballard, 1991, Sutton and Barto, 2018]. Moreover, without flow feedback, the agent is capable of learning a strong drag-minimizing, approximately sinusoidal action sequence, and in Section C we show that a closely related sequence from the same parameterized family substantially increases drag, yet the agent fails to discover it. We also observe that without flow feedback, multiple standard model-free off-policy and on-policy RL algorithms (from the stable implementations of Raffin et al. [2021]) fail, at least without careful hyperparameter tuning; see Section E.4. Instead, we observe that a key difference between the drag-maximization and drag-minimization tasks is that, in drag maximization, early measurements *anti-align* with long-run performance: substantially *increasing* drag requires control actions that initially *decrease* drag; see Figure 5. This behavior can be motivated by boundary-layer separation: impulsive rotation energizes the advancing-side boundary layer and delays separation while promoting earlier separation on the retreating side, leading to a net decrease in measured drag [Badr and Dennis, 1985, Badr et al., 1990, Aljure Osorio et al., 2014]. Such deceptive transients are characteristic of many non-minimum-phase systems, including bicycle steering [Åström et al., 2005], walking [Dallali et al., 2009, Wee et al., 2013], and VTOL/CTOL aircraft [Hauser et al., 1992]. Recent work emphasizes the difficulties in learning to control non-minimum-phase systems and motivates ad hoc fixes [Charfeddine et al., 2025, Agyei et al., 2025, van Zundert and Oomen, 2018, Zhou et al., 2018]; see also Section 4.2.

In contrast, our experiments show that in a complex physical system a generalist RL agent can overcome the increased learning difficulties related to deceptive initial transients purely by enriching its observations during training.

4 Discussion

Beyond drag control, our findings speak to the role of privileged information in RL, the selective use of feedback, and the value of observations for learning to control.

4.1 Privileged information and observation-adaptive agents

The relevance of different observations at training and deployment has been recognized in both supervised learning and RL. In supervised learning, Vapnik et al. [2015] formalized *learning using privileged information*, where additional inputs are available only at training time. In RL, asymmetric actor-critic and related distillation methods [Pinto et al., 2017, Chen et al., 2020, Salter et al., 2021, Ma et al., 2023, Baladron et al., 2023] use low-dimensional, clean, or simulator-only state (often with bottlenecks and domain randomization [Pinto et al., 2017]) to speed up or stabilize training of a policy that ultimately operates from higher-dimensional, noisy sensors, largely motivated by the convenience of simulation. Our results point to a complementary regime. In our setup, learning the drag-maximizing policy appears to require *more* information during training than at execution. More generally, techniques viable only in simulation clash with the goal of understanding the process of human-like skill acquisition. Recent sensory-scaffolding work [Hu et al., 2024] is conceptually close, using privileged sensing to train world models and critics that support policies with simpler (often cheaper) observations at deployment time. However, this relies on specialized architectures and a fixed split between training-time and deployment-time sensors. In

contrast, our results suggest that an agent should be able to call on feedback when needed to extract the remaining gains in performance.

There is also a growing body of work in control and reinforcement learning where agents decide *when* to use observations rather than treating sensing as fixed. Examples include RL for event-triggered feedback control [Baumann et al., 2018], in which control actions are applied at endogenously determined events rather than on a fixed clock, and RL with costly optional observations [Holt et al., 2023, Nam et al., 2021, Bellinger et al., 2023], in which the learner trades off the information content of an observation against an explicit cost of acquiring it. Our experimental results suggest a subtly different regime: we are interested in settings where observations arrive anyway, but the agent can learn to selectively ignore them. This may be a better choice when the observations are uninformative or too noisy. In some scenarios, they may be not worth the additional computation. In certain cases, the internal state and inference-time requirements of the maneuver may render predominantly open-loop (or, more generally, feedforward [Åström and Murray, 2021]) strategy preferable. On the other hand, the agent may want to emphasize them when they materially improve control. In such settings, assigning an artificial sensing cost may bias the learned strategies. To our knowledge, this “use-when-useful” regime remains largely unexplored.

Observation-adaptive agents. Although we do not propose a new architecture here, our results suggest the following high-level desiderata:

- (i) rely primarily on internal state and open-loop structure when confident;
- (ii) increase the use of high-dimensional sensors when uncertainty grows or when small deviations have large consequences; and
- (iii) gradually reduce this reliance as internal models improve, without a fixed split between training-time and deployment-time observations.

The Kalman filter [Kalman, 1960] provides a clean instance of the adaptive mechanism we are hinting at: as state uncertainty shrinks, the gain on measurements automatically decreases. Analogously, we envision generalist RL agents that *learn when* rich feedback is worth using, rather than having their sensor sets hard-wired by the designer; for instance, using the paradigm of options Sutton et al. [2022]. This shifts the focus away from designing separate networks for different observation sets and toward mechanisms that avoid information overload and allocate compute and attention efficiently, yet remain adaptable—closer to how organisms navigate an abundance of sensory stimuli while relying on automatized skills most of the time.

4.2 Quantifying the value of feedback for learning

Classical control theory emphasizes limits imposed by the observation process on *robust execution*, from linear-quadratic-Gaussian results [Doyle, 2003] to studies of stick balancing and learned controllers [Leong and Doyle, 2016, Xu et al., 2021] (coincidentally, all non-minimum-phase systems). Our experiments point to a complementary notion: the *value of feedback for exploration*, even when feedback is not needed to execute the final policy. In our setup, restricted observations are sufficient for control in the usual sense—we know that good open-loop policies exist and we rule out simple forms of state aliasing—yet certain tasks exhibit systematic learning failures without flow feedback. This places our system outside the regimes where partial observability is provably benign [Liu et al., 2022]: the issue is not the existence of a good policy, but the reliability with which a general-purpose learner can discover it under different observation modalities. Lee et al. [2024] show that the extra cost incurred by a controller learned from data grows with how sensitive the optimal performance is to errors in the system parameters, and shrinks with how informative the data are about those parameters. We speculate that access to flow feedback

increases information along control-relevant directions, enabling more accurate models, more efficient exploration, and overall a less fragile learning process.

5 Conclusion

We summarize our main contributions, limitations, and directions for future work.

Contributions. We study how feedback shapes the learning of open-loop policies by interfacing a generalist RL agent directly with the chaotic flow around a spinning cylinder in our water-channel setup. By selectively providing or withholding flow measurements during training, we isolate the role of external flow feedback in learning. Our results on the drag-maximization task support a simple principle, backed by real-world experiments on a chaotic flow: learning a skill can require substantially richer information than executing it. In our case, high-dimensional flow feedback is indispensable for learning a good drag-maximizing policy, yet unnecessary to execute it. In contrast, drag minimization appears to require little detailed feedback during training. We trace this asymmetry to dynamic systems theory and the concept of non-minimum-phase behavior. In particular, the same physical system presents kind or wicked learning conditions depending solely on the goal, not on dynamics and policy complexity. More broadly, our experiments illustrate how generalist reinforcement learning agents can serve as scientific instruments to probe how skills are acquired in rich physical environments, and motivate architectures that selectively use feedback during both training and deployment. Beyond this conceptual point, we also contribute to the fluids-control literature (see Section B). Most notably, we recover a high-performance policy within minutes of real-world interaction, compared to the hours of simulation time required by prior work on shorter tasks. While such tuned simulations provide useful intuition and a consistency check, they inevitably depend on modeling and parameter choices; our results instead demonstrate that the desired behavior can be learned directly from interaction with the underlying flow.

Limitations. Our results are limited to a single physical setup, but our analysis suggests that the phenomena may extend to other nonlinear non-minimum-phase systems. Our methodology is broadly applicable, and exploring additional physical systems is an interesting direction for future work.

Outlook. On the theoretical side, an important next step is to analyze simplified models that clarify when rich feedback is needed for learning but not for execution, and to derive principled rules for choosing observations. Such a framework could guide the design of RL agents that decide when and where to “look”, basing their decisions on informative measurements rather than fixed sensor sets; see Section 4. Beyond our water-channel setup, these phenomena should be tested on other platforms. The setup of Bi and D’Andrea [2024] is a promising second system, and high-dimensional robots such as humanoids are a natural longer-term target. A key challenge is to disentangle the roles of open-loop (or more generally feedforward) patterns and feedback. As RL models improve, they can increasingly serve as scientific instruments to probe skill acquisition and, ultimately, human learning. Finally, our platform opens several directions for fluids control: benchmarking continual learning algorithms [Sutton et al., 2022], controlling more complex shapes in challenging or adversarial flow conditions, benchmarking sensor-placement strategies (e.g., selecting a small subset of flow measurements), and evaluating algorithms that exploit privileged or asymmetric observations.

Acknowledgments. We are grateful to all the colleagues who discussed this work with us and were intrigued by our setup. In particular, we thank F. Noca and R. Bernhard for feedback on the fluid-dynamics hardware, A. K. Marcus, M. M. Felix, and D. Wagner for help with electronics and fabrication, T. Bi for the raw pictures of the setup, B. Lee for the discussions on limits of learning to control, and N. Lanzetti, S. Bolognani, and P. Grontas for their curiosity and insightful comments.

References

- Amir H Abdi, Benedikt Sagl, Venkata P Srungarapu, Ian Stavness, Eitan Prisman, Purang Abolmaesumi, and Sidney Fels. Characterizing motor control of mastication with soft actor-critic. *Frontiers in Human Neuroscience*, 2020.
- David J Acheson. *Elementary fluid dynamics*. Oxford University Press, 1990.
- Jack A Adams. A closed-loop theory of motor learning. *Journal of Motor Behavior*, 1971.
- Klinsmann Agyei, Pouria Sarhadi, and Daniel Polani. Deep reinforcement learning in applied control: Challenges, analysis, and insights. *arXiv preprint arXiv:2507.08196*, 2025.
- Md Mahbub Alam. Flow-induced vibrations of various bluff bodies: a review of blockage and wall effects. *Journal of Fluids and Structures*, 136:104328, 2025.
- David E Aljure Osorio, Ivette María Rodríguez Pérez, Oriol Lehmkuhl Barba, Carlos David Pérez Segarra, and Asensio Oliva Llena. Influence of rotation on the flow over cylinder at $Re = 5000$. In *ETMM10-10th International ERCOFTAC Symposium on Engineering Turbulence Modelling and Measurements*, 2014.
- David I Anderson, Minxuan He, Paula Gutierrez, Ichiro Uchiyama, and Joseph J Campos. Do balance demands induce shifts in visual proprioception in crawling infants? *Frontiers in Psychology*, 2019.
- Karl Johan Åström and Richard Murray. *Feedback systems: an introduction for scientists and engineers*. Princeton university press, 2021.
- Karl Johan Åström, Richard E Klein, and Anders Lennartsson. Bicycle dynamics and control. *Control Systems Magazine*, 2005.
- HM Badr and SCR Dennis. Time-dependent viscous flow past an impulsively started rotating and translating circular cylinder. *Journal of Fluid Mechanics*, 1985.
- HM Badr, M Coutanceau, SCR Dennis, and C Menard. Unsteady flow past a rotating circular cylinder at Reynolds numbers 103 and 104. *Journal of Fluid Mechanics*, 1990.
- Javier Baladron, Julien Vitay, Torsten Fietzek, and Fred H Hamker. The contribution of the basal ganglia and cerebellum to motor learning: A neuro-computational approach. *PLOS Computational Biology*, 2023.
- Francesco Banelli, Antonio Terpin, Alan Bonomi, and Raffaello D’Andrea. Flow gym. *Working paper*, 2025.
- Dominik Baumann, Jia-Jie Zhu, Georg Martius, and Sebastian Trimpe. Deep reinforcement learning for event-triggered control. In *2018 IEEE Conference on Decision and Control (CDC)*, 2018.

- Colin Bellinger, Mark Crowley, and Isaac Tamblyn. Dynamic observation policies in observation cost-sensitive reinforcement learning. *arXiv preprint arXiv:2307.02620*, 2023.
- Thomas Bi and Raffaello D’Andrea. Sample-efficient learning to solve a real-world labyrinth game using data-augmented model-based reinforcement learning. In *IEEE International Conference on Robotics and Automation*, 2024.
- Noam Brown and Tuomas Sandholm. Superhuman AI for multiplayer poker. *Science*, 2019.
- Monia Charfeddine, Khalil Jouili, and Mongi Ben Moussa. Adaptive control of nonlinear non-minimum phase systems using actor–critic reinforcement learning. *Symmetry*, 2025.
- Michail Chatzimanolakis, Pascal Weber, and Petros Koumoutsakos. Drag reduction in flows past 2D and 3D circular cylinders through deep reinforcement learning. *arXiv preprint arXiv:2309.02109*, 2023.
- Chi-Tsong Chen. *Analog and digital control system design: transfer-function, state-space, and algebraic methods*. Oxford University Press, Inc., 1995.
- Dian Chen, Brady Zhou, Vladlen Koltun, and Philipp Krähenbühl. Learning by cheating. In *Conference on robot learning*, 2020.
- Haecheon Choi, Parviz Moin, and John Kim. Active turbulence control for drag reduction in wall-bounded flows. *Journal of Fluid Mechanics*, 1994.
- Christopher J Clark and Richard O Prum. Aeroelastic flutter of feathers, flight and the evolution of non-vocal communication in birds. *Journal of Experimental Biology*, 2015.
- Luca Cortelezzi, JL Speyer, KH Lee, and J Kim. Robust reduced-order control of turbulent channel flows via distributed sensors and actuators. In *IEEE Conference on Decision and Control (CDC)*, 1998.
- Madeleine Coutanceau and Christian Menard. Influence of rotation on the near-wake development behind an impulsively started circular cylinder. *Journal of Fluid Mechanics*, 1985.
- Jared S Cox, Kenneth S Brentner, and Christopher L Rumsey. Computation of vortex shedding and radiated sound for a circular cylinder: subcritical to transcritical reynolds numbers. *Theoretical and Computational Fluid Dynamics*, 1998.
- Houman Dallali, Martin Brown, and Bram Vanderborght. Using the torso to compensate for non-minimum phase behaviour in ZMP bipedal walking. In *Advances in Robotics Research: Theory, Implementation, Application*. Springer, 2009.
- Robert Dorfman, Paul Anthony Samuelson, and Robert M Solow. *Linear programming and economic analysis*. Courier Corporation, 1987.
- John Doyle. Guaranteed margins for LQG regulators. *IEEE Transactions on automatic Control*, 2003.
- MA Elhawary. Deep reinforcement learning for active flow control around a circular cylinder using unsteady-mode plasma actuators. *arXiv preprint arXiv:2012.10165*, 2020.
- Takahide Endo, Nobuhide Kasagi, and Yuji Suzuki. Feedback control of wall turbulence with wall deformation. *International Journal of Heat and Fluid Flow*, 2000.

- Michele Garibbo, Casimir Ludwig, Nathan Lepora, and Laurence Aitchison. What deep reinforcement learning tells us about human motor learning and vice-versa. *arXiv preprint arXiv:2208.10892*, 2022.
- Hassan Ghraieb, Jonathan Viquerat, Aurélien Larcher, Philippe Meliga, and Elie Hachem. Single-step deep reinforcement learning for open-loop control of laminar and turbulent flows. *Physical Review Fluids*, 2021.
- Tuomas Haarnoja, Aurick Zhou, Pieter Abbeel, and Sergey Levine. Soft actor-critic: Off-policy maximum entropy deep reinforcement learning with a stochastic actor, 2018.
- Danijar Hafner, Jurgis Pasukonis, Jimmy Ba, and Timothy Lillicrap. Mastering diverse control tasks through world models. *Nature*, 2025.
- John Hauser, Shankar Sastry, and George Meyer. Nonlinear control design for slightly non-minimum phase systems: Application to V/STOL aircraft. *Automatica*, 1992.
- Samuel Holt, Alihan Hüyük, and Mihaela van der Schaar. Active observing in continuous-time control. *Advances in Neural Information Processing Systems*, 36:46054–46092, 2023.
- Edward S Hu, James Springer, Oleh Rybkin, and Dinesh Jayaraman. Privileged sensing scaffolds reinforcement learning. *arXiv preprint arXiv:2405.14853*, 2024.
- Marco Iosa, Augusto Fusco, Giovanni Morone, and Stefano Paolucci. Walking there: environmental influence on walking-distance estimation. *Behavioural Brain Research*, 2012.
- Javier Jiménez. Turbulent flows over rough walls. *Annu. Rev. Fluid Mech.*, 36(1):173–196, 2004.
- Rudolph Emil Kalman. A new approach to linear filtering and prediction problems. 1960.
- Shoko Kasuga, Sebastian Telgen, Junichi Ushiba, Daichi Nozaki, and Jörn Diedrichsen. Learning feedback and feedforward control in a mirror-reversed visual environment. *Journal of Neurophysiology*, 2015.
- Till Kroeger, Radu Timofte, Dengxin Dai, and Luc Van Gool. Fast optical flow using dense inverse search. In *European conference on computer vision*, 2016.
- Bruce D Lee, Ingvar Ziemann, George J Pappas, and Nikolai Matni. Active learning for control-oriented identification of nonlinear systems. In *2024 IEEE 63rd Conference on Decision and Control (CDC)*, 2024.
- Changhoon Lee, John Kim, David Babcock, and Rodney Goodman. Application of neural networks to turbulence control for drag reduction. *Physics of Fluids*, 1997.
- Changhoon Lee, John Kim, and Haecheon Choi. Suboptimal control of turbulent channel flow for drag reduction. *Journal of Fluid Mechanics*, 1998.
- David N Lee and Eric Aronson. Visual proprioceptive control of standing in human infants. *Perception & Psychophysics*, 1974.
- Yoke Peng Leong and John C Doyle. Understanding robust control theory via stick balancing. In *2016 IEEE 55th Conference on Decision and Control (CDC)*, 2016.
- Qinghua Liu, Alan Chung, Csaba Szepesvári, and Chi Jin. When is partially observable reinforcement learning not scary? In *Conference on Learning Theory*, 2022.

- Hao Ma, Dieter Büchler, Bernhard Schölkopf, and Michael Muehlebach. Reinforcement learning with model-based feedforward inputs for robotic table tennis. *Autonomous Robots*, 2023.
- Laura A Malone, Nayo M Hill, Haley Tripp, Vadim Zipunnikov, Daniel M Wolpert, and Amy J Bastian. The control of movement gradually transitions from feedback control to feedforward adaptation throughout childhood. *npj Science of Learning*, 2025.
- Lionel Mathelin, Mohamed Abbas-Turki, Luc Pastur, and Hisham Abou-Kandil. Closed-loop fluid flow control using a low dimensional model. *Mathematical and Computer Modelling*, 2010.
- Tad McGeer et al. Passive dynamic walking. *International Journal of Robotics Research*, 1990.
- S Mittal. Control of flow past bluff bodies using rotating control cylinders. *Journal of Fluids and Structures*, 2001.
- S Mittal. Flow control using rotating cylinders: effect of gap. *Journal of Applied Mechanics*, 2003.
- Tirtsä Naaman, Roei Hayek, Itai Gutman, and Shmuel Springer. Young, but not in the dark—the influence of reduced lighting on gait stability in middle-aged adults. *PLOS ONE*, 2023.
- Hyunji Alex Nam, Scott Fleming, and Emma Brunskill. Reinforcement learning with state observation costs in action-contingent noiselessly observable markov decision processes. *Advances in Neural Information Processing Systems*, 2021.
- Christoffer Norberg. Effect of reynolds number and a low-intensity freestream turbulence on the flow around a circular cylinder. 1987.
- Daniel Palenicek, Theo Gruner, Tim Schneider, Alina Böhm, Janis Lenz, Inga Pfenning, Eric Krämer, and Jan Peters. Learning tactile insertion in the real world. *arXiv preprint arXiv:2405.00383*, 2024.
- Romain Paris, Samir Beneddine, and Julien Dandois. Robust flow control and optimal sensor placement using deep reinforcement learning. *Journal of Fluid Mechanics*, 2021.
- Lerrel Pinto, Marcin Andrychowicz, Peter Welinder, Wojciech Zaremba, and Pieter Abbeel. Asymmetric actor critic for image-based robot learning. *arXiv preprint arXiv:1710.06542*, 2017.
- Jean Rabault, Miroslav Kuchta, Atle Jensen, Ulysse Réglade, and Nicolas Cerardi. Artificial neural networks trained through deep reinforcement learning discover control strategies for active flow control. *Journal of Fluid Mechanics*, 2019.
- Antonin Raffin, Ashley Hill, Adam Gleave, Anssi Kanervisto, Maximilian Ernestus, and Noah Dormann. Stable-baselines3: Reliable reinforcement learning implementations. *Journal of Machine Learning Research*, 2021.
- Adi Raichin, Anat Shkedy Rabani, and Lior Shmuelof. Motor skill training without online visual feedback enhances feedforward control. *Journal of Neurophysiology*, 2021.
- Feng Ren, Jean Rabault, and Hui Tang. Applying deep reinforcement learning to active flow control in weakly turbulent conditions. *Physics of Fluids*, 2021.
- Angel Romero, Ashwin Shenai, Ismail Geles, Elie Aljalbout, and Davide Scaramuzza. Dream to fly: Model-based reinforcement learning for vision-based drone flight. *arXiv preprint arXiv:2501.14377*, 2025.

- Sasha Salter, Dushyant Rao, Markus Wulfmeier, Raia Hadsell, and Ingmar Posner. Attention-privileged reinforcement learning. In *Conference on Robot Learning*, 2021.
- Richard A Schmidt. A schema theory of discrete motor skill learning. *Psychological Review*, 1975.
- Julian Schrittwieser, Ioannis Antonoglou, Thomas Hubert, Karen Simonyan, Laurent Sifre, Simon Schmitt, Arthur Guez, Edward Lockhart, Demis Hassabis, Thore Graepel, et al. Mastering atari, go, chess and shogi by planning with a learned model. *Nature*, 2020.
- John Schulman, Filip Wolski, Prafulla Dhariwal, Alec Radford, and Oleg Klimov. Proximal policy optimization algorithms, 2017.
- Jan L Souman, Ilja Frissen, Manish N Sreenivasa, and Marc O Ernst. Walking straight into circles. *Current Biology*, 2009.
- Venkata Praneeth Srungarapu. *Reinforcement learning of a feedforward controller with soft actor-critic for a reaching task*. PhD thesis, University of British Columbia, 2021.
- Pol Suárez, Francisco Álcantara-Ávila, Jean Rabault, Arnau Miró, Bernat Font, Oriol Lehmkuhl, and Ricardo Vinuesa. Flow control of three-dimensional cylinders transitioning to turbulence via multi-agent reinforcement learning. *arXiv preprint arXiv:2405.17210*, 2024.
- Richard S Sutton and Andrew G Barto. *Reinforcement learning: An introduction*. MIT press, 2018.
- Richard S Sutton, Michael Bowling, and Patrick M Pilarski. The alberta plan for AI research. *arXiv preprint arXiv:2208.11173*, 2022.
- Hongwei Tang, Jean Rabault, Alexander Kuhnle, Yan Wang, and Tongguang Wang. Robust active flow control over a range of reynolds numbers using an artificial neural network trained through deep reinforcement learning. *Physics of Fluids*, 2020.
- Antonio Terpin, Alan Bonomi, Francesco Banelli, and Raffaello D'Andrea. Synthpix: A lightspeed PIV images generator. *Working paper*, 2025.
- Mikhail Tokarev, Egor Palkin, and Rustam Mullyadzhanov. Deep reinforcement learning control of cylinder flow using rotary oscillations at low Reynolds number. *Energies*, 2020.
- PT Tokumar and PE Dimotakis. Rotary oscillation control of a cylinder wake. *Journal of Fluid Mechanics*, 1991.
- PT Tokumar and PE Dimotakis. The lift of a cylinder executing rotary motions in a uniform flow. *Journal of Fluid Mechanics*, 1993.
- Jurgen van Zundert and Tom Oomen. On inversion-based approaches for feedforward and ilc. *Mechatronics*, 2018.
- Vladimir Vapnik, Rauf Izmailov, et al. Learning using privileged information: Similarity control and knowledge transfer. *J. Mach. Learn. Res.*, 2015.
- Teck-Chew Wee, Alessandro Astolfi, and Xie Ming. The design and control of a bipedal robot with sensory feedback. *International Journal of Advanced Robotic Systems*, 2013.

- Steven D Whitehead and Dana H Ballard. Learning to perceive and act by trial and error. *Machine Learning*, 1991.
- Hui Xu, Wei Zhang, Jian Deng, and Jean Rabault. Active flow control with rotating cylinders by an artificial neural network trained by deep reinforcement learning. *Journal of Hydrodynamics*, 2020.
- Jingxi Xu, Bruce Lee, Nikolai Matni, and Dinesh Jayaraman. How are learned perception-based controllers impacted by the limits of robust control? In *Learning for Dynamics and Control*, 2021.
- Minghui Ye and Ahmed H Elsheikh. Model-based reinforcement learning for active flow control. *Physics of Fluids*, 37(9), 2025.
- Siqi Zhou, Mohamed K Helwa, and Angela P Schoellig. An inversion-based learning approach for improving impromptu trajectory tracking of robots with non-minimum phase dynamics. *IEEE Robotics and Automation Letters*, 2018.
- Zisong Zhou, Mengqi Zhang, and Xiaojue Zhu. Reinforcement-learning-based control of turbulent channel flows at high reynolds numbers. *Journal of Fluid Mechanics*, 2025.

A A tabletop circulating water channel (CWC)

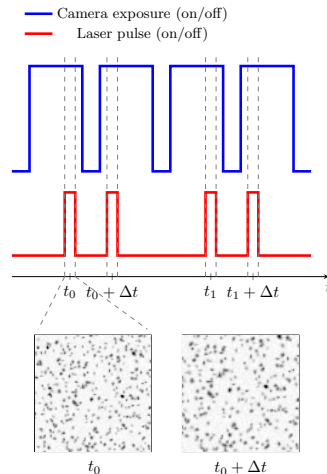
Figure 2 illustrates the tabletop CWC, with close-ups and labels for all components. The mean incoming flow speed at the beginning of the test section is regulated to 0.12 m/s . All off-the-shelf parts are listed below; the others are 3D-printed, and their designs are available on the project website. The entire setup fits inside a $0.9 \times 0.3 \times 0.3 \text{ m}^3$ Long Aquarium (90 L, Olibetta), with a test section of $0.15 \times 0.10 \times 0.15 \text{ m}^3$ —much smaller than typical water channels used in fluids-control studies.

Recirculating water channel. The channel consists of an upper and a lower branch. The test section (1) in the upper branch houses the cylinder (2). Three APISQUEEN U5 brushless propellers (3) drive a left-to-right flow, which is redirected into the lower branch by guide vanes (4) and then back to the upper branch. A honeycomb structure (5) straightens the flow and suppresses large-scale vortices. Flow restrictions (6) accelerate the stream and stretch remaining small-scale vortices. The particle image velocimetry (PIV) setup (7) captures images at 60 Hz, which are used to estimate the flow field in real time by exploiting hardware acceleration [Banelli et al., 2025].

Cylinder actuation. The cylinder (2) is the controlled object of the setup and is attached to a Maxon EC45 flat motor with a 640 PPR incremental encoder. The cylinder radius is $R = 0.021 \text{ m}$. We cap the rotation rate at $\dot{A} = 15.7 \text{ rad/s}$, which corresponds to imposing a surface flow speed of about 0.33 m/s , more than twice the average incoming flow speed, so that the actuation can locally reverse the flow. Given a crude upper bound for the characteristic frequency, $f_c \leq 1.5 \text{ Hz}$ (obtained using $\text{St} \leq 0.32$ for the Strouhal number [Cox et al., 1998], an inflow speed $U_\infty \leq 0.2 \text{ m/s}$, and $f_c = \text{St}U_\infty/D$), we adopt a sampling frequency for the control input of 30 Hz, which comfortably satisfies standard guidelines from sampled-data control and signal processing [Chen, 1995].

Drag measurements. The motor is mounted on a shaft at \vec{x}_0 , parallel to the flow surface and transverse to the incoming flow. Torque about this shaft is measured with a TD50 150 mNm sensor by ME-Meßsysteme GmbH (2), with full scale 150 mNm and accuracy 0.1% of full scale. The measured signal $\hat{\tau}_{\text{drag}}^m(t)$ is a noisy estimate of the torque $\tau_{\text{drag}}(t)$ and an indirect measurement of the drag force in the direction of the flow \vec{n}_∞ . Throughout this work, we refer to drag and torque measurements interchangeably. We sample $\hat{\tau}_{\text{drag}}^m(t)$ at a rate of 1 kHz, and smooth it by averaging over the last second of data. This standard practice in flow control reduces sensor noise and vortex-shedding fluctuations, without affecting our learning objective, which depends on average performance over a fixed time interval $T = 60 \text{ s}$. We verify the quality of the torque measurements in Section D.2. The no-control baseline is computed as the average, across all experiments, of the initial measured torque. In our experiments, it amounts to 82.64 mNm .

Flow feedback. To estimate the flow field around the cylinder, we use PIV, which is one of the most important modalities for quantifying flow fields in bluff body wakes. For this, we use the low-cost PIV system provided by Optolution (7). In PIV, laser pulses illuminate neutrally buoyant particles in the fluid through the transparent acrylic section in the middle of the flow restrictions at specific intervals, while the camera captures images. We use $10\text{ }\mu\text{m}$ -diameter hollow glass spheres (LaVision) as tracer particles. The plot on the right depicts the timing sequence of camera exposure (blue line, top) and laser pulses (red line, below). The bottom part of the figure shows two consecutive particle images taken at times t_0 and $t_0 + \Delta t$. These (in our setup, 1 megapixel) images are used to track the particle displacement and estimate the velocity fields; see Section D.3 for more details on our pipeline. Examples of flow estimates are reported in Figure 2.



Computational resources. Data are collected on an Ubuntu 22.04 machine with an AMD Ryzen Threadripper PRO 5995WX and four Nvidia RTX 4090 GPUs. One GPU is used for computing the flow estimate, one GPU for policy inference and one for training.

B Related work in fluids control

Although our work is not about flow control per se, we adopt it as a demanding testbed because it concentrates exactly the properties we seek to study, namely the interplay between open-loop actuation and feedback corrections in learning. Using this setting lets us probe how generalist RL agents build and exploit internal world models while remaining grounded in a physically rich, externally verifiable environment. In this appendix, we therefore acknowledge the fluids-control literature that informs and contextualizes our study. At the same time, our contribution intersects with that field: to our knowledge, we are the first to interface RL with real-time, full-flow feedback from PIV at high frequency, enabling closed-loop learning directly from real-world flow measurements.

Challenges. The task of fluids control comes with several challenges:

- (i) Lack of standard benchmarks and testbeds in the physical world (traditional water channels are costly and designed for fluid analysis rather than control).
- (ii) Unlike most control applications, the underlying system considered is infinite-dimensional, extremely difficult to model accurately, and slow to simulate. Until recently, only low-dimensional model approximations were feasible due to computational constraints.
- (iii) Past limitations in computing resources restricted the information available to feedback policies. To the best of our knowledge, we are the first to provide real-time flow estimates as feedback to the control policy.

We tackle these challenges by designing and openly releasing an affordable tabletop recirculating water channel, which we describe in Section A, and by heavily exploiting parallelism on accelerators for fluid

flow estimation, retaining accuracy while reducing computational time.

Why now? The pioneers in this field were prevented from effectively exploiting closed-loop control techniques because of the limited computational resources available. For this, they resorted to open-loop strategies [Coutanceau and Menard, 1985, Tokumar and Dimotakis, 1991, 1993, Mittal, 2001, 2003], low-dimensional models [Cortelezzi et al., 1998, Mathelin et al., 2010], low-dimensional measurements with simple proportional control strategies (e.g., wall pressure measurements for near-wall turbulence reduction [Choi et al., 1994, Lee et al., 1998, Endo et al., 2000]) or shallow neural networks [Lee et al., 1997]. In recent years, unprecedented computing power became more accessible in the consumer market. Importantly, these resources enable real-time, computationally intensive control techniques for previously intractable high-dimensional systems. Among these, RL has excelled in a variety of control tasks, even in tasks traditionally mastered only by humans [Schrittwieser et al., 2020, Brown and Sandholm, 2019]. Naturally, these techniques rippled into the fluids-control domain [Rabault et al., 2019, Elhawary, 2020, Tokarev et al., 2020, Paris et al., 2021, Ren et al., 2021, Ghraieb et al., 2021, Tang et al., 2020, Xu et al., 2020, Chatzimanolakis et al., 2023, Suárez et al., 2024, Zhou et al., 2025, Ye and Elsheikh, 2025]. However, most of this work has only been done in simulation.

Why are simulations not sufficient? In this work, we synthesize a control policy using RL, skipping simulation altogether and instead training the policy directly on a physical setup. Several reasons motivate our physical-only approach:

- Fluid simulations are hard to calibrate and highly sensitive to modeling errors, especially in complex environments, with an inevitable sim-to-real gap. As an example, with a cylinder diameter $D = 0.042$ m the Reynolds number is $Re = \frac{U_\infty D}{\nu} \approx 5.0 \times 10^3$, which lies in the subcritical vortex-shedding regime for circular cylinders [Norberg, 1987]. The distance between the walls is approximately 0.1 m and, thus, the blockage ratio is $BR = D/H \approx 0.42$ [Alam, 2025]. Then, walls have significant impact on the cylinder wake [Jiménez, 2004] and should be carefully modeled.
- They are often computationally expensive and slow, making real-time training or adaptation impractical. For this, one has to resort to simplifications. Even then, a few seconds of simulation time may require a full day of calculations on a consumer setup.
- More broadly, simulations generally fail to capture subtle physical effects that significantly impact control—consider, for example, the aeroelasticity of feathers, surface wetting, or micro-vortex interactions; see, e.g., the work of Clark and Prum [2015].

Contributions to the fluids-control literature. Our contributions to the fluids-control community are four-fold. First, we design and release an open-source, low-cost tabletop CWC as a versatile experimental testbed. We believe that this testbed can become the standard for rapidly prototyping and experimenting with flow control techniques and interfacing RL to flow control problems. Second, we demonstrate, for the first time, the deployment of reinforcement learning with full-field, high-resolution flow feedback, executed directly online on the physical system. Importantly, we show that this results in extremely sample-efficient learning. In comparison, the most recent result—from Ye and Elsheikh [2025]—of RL in fluids control (performed without high-resolution flow feedback and in a two-dimensional simulation) requires several hours (~ 10) for two-second episodes (80 steps). To perform this experiment, we exploited GPU programming and developed an optical flow algorithm to estimate flow fields with accuracy acceptable by flow-measurement standards, while occupying only a fraction of the computational budget

of the control pipeline [Banelli et al., 2025]. In doing so, we also developed a software package for generating synthetic PIV images orders of magnitude faster than existing methods [Terpin et al., 2025]. This allowed us to iterate quickly on the flow-estimation algorithms and we believe the community will benefit from it. Third, by investigating the reasons behind the lack of learning in the drag-maximization task, we discuss the non-minimum-phase properties of the vortex-shedding phenomena behind a cylinder, connecting our conclusions to boundary-layer theory. To our knowledge, this observation is novel and our learning results underscore its relevance for fluids-control applications.

C The performance of open-loop control

In this section, we describe our procedure to verify that simple sinusoidal open-loop inputs can achieve high performance and to identify representative high-performing sinusoids for both drag maximization and drag minimization. Note that, for the scope of our work and claims, it is not important to find the globally best open-loop policy, or even the best sinusoidal one; it suffices to obtain a high-performing policy. We systematically probe the system with open-loop policies of the form $\omega(t) = A \sin(2\pi ft)$, $A \in [0, 15.700] \text{ rad/s}$ and $f \in [0, 3] \text{ Hz}$. The no-control baseline corresponds to $A = 0$ (zero actuation). We restrict $f \in [0, 3] \text{ Hz}$ given our 30 Hz actuation rate, which ensures at least ten control updates per period Chen [1995]. We sweep over a grid of amplitudes ($A \in \{7.85, 10.467, 13.083, 15.700\} \text{ rad/s}$) and frequencies (values spaced by 0.1 Hz) to efficiently identify promising regions in the parameter space. For each combination, we collect three repetitions and compute the mean performance, observing fairly consistent outcomes across repetitions. This first search suggests the candidates ($A = 15.700 \text{ rad/s}$, $f = 0.8 \text{ Hz}$) for drag maximization and ($A = 15.700 \text{ rad/s}$, $f = 3.0 \text{ Hz}$) for drag minimization, with performance plateauing for $f > 2.5 \text{ Hz}$. Since the minimizing frequency lies at the upper boundary of the initial scan, we empirically verified that performance for $f > 3.0 \text{ Hz}$ changes by less than 2% relative to the no-control baseline and eventually degrades due to poor tracking and sampling limitations at higher frequencies. The best amplitude is also found at the upper boundary, $A = 15.700 \text{ rad/s}$, but this limit is imposed also on the RL agent and is physically justified; see Section A. Moreover, increasing the amplitude further leads to action trajectories that excite strong surface waves in the water channel and amplify boundary effects, so we do not consider larger amplitudes. Given the outcome of this first search, we fix the drag-minimizing policy to ($A = 15.700 \text{ rad/s}$, $f = 3.0 \text{ Hz}$). For drag maximization, we fix $A = 15.700 \text{ rad/s}$ and further refine the frequency by performing five steps of ternary search over $f \in [0.71, 0.89] \text{ Hz}$, computing the performance of each frequency as the average over five repetitions. Overall, we pick as high-performance sinusoidal strategies ($A = 15.700 \text{ rad/s}$, $f = 0.776 \text{ Hz}$) for drag maximization and ($A = 15.700 \text{ rad/s}$, $f = 3.0 \text{ Hz}$) for drag minimization. We collect ten repetitions of each policy and use the mean performance as the open-loop baseline for the two tasks, obtaining an increase of about 28% in drag for the maximization task and a decrease of about 32% for the minimization task relative to the no-control baseline.

D Additional information on the data acquisition pipeline

In this section, we include additional information on the data acquisition pipeline.

D.1 Additional sources of uncertainty

In our experiments, we recognize that several secondary sources of uncertainty can influence the data. For instance, the uncertainties due to the torque sensor measurements are below 0.15 mNm and the ones related to non-idealities in the fabrication and assembly are below 0.6 mNm for the cylinder; see Section D.2. Other sources of uncertainty include natural variations in room temperature, small fluctuations in the water level, and minor mechanical non-idealities, such as slightly different tracking performance on the desired speed of the propellers. These effects may introduce small discrepancies in the results, but their overall effect is limited. Importantly, we deliberately avoid drawing conclusions from changes of only a few percent. Instead, our analysis focuses on robust effects of clear significance, for which these small sources of variability are inconsequential. Finally, since we collect data over multiple weeks, the no-control baseline shows minor variations across experiments. This bias, for instance due to temperature changes, is minor, and we systematically remove it by considering changes in torque measurements rather than their absolute values.

D.2 Additional experiment to verify that the cylinder dynamics are inconsequential for the torque sensor measurements

To verify that our torque sensor is not contaminated by the actuation itself, we performed a dedicated characterization. Because the motor is mounted on the same shaft as the sensor, the motor dynamics together with misalignment (due to, e.g., fabrication inaccuracies) of the center of mass of the cylinder with respect to the rotational axis could, in principle, affect the measured torque. We therefore designed a simple experiment to bound any actuation-induced artifacts under representative operating conditions.

Experimental setup. In a quiescent, no-flow environment, we command the cylinder to track open-loop sinusoidal profiles over the same grid of amplitudes and frequencies as in Section C. For each grid point, we collect 60s of data and repeat the experiment 3 times.

Results. Overall, the measured torque values belong to the range $[-0.48, 0.56]\text{ mNm}$. Thus, it is clear that the conclusions in Section 3 are not affected by these parasitic effects.

D.3 Additional details on the vision pipeline

While the Optolution PIV system yields high-quality, high-resolution image pairs, it does not provide real-time processing and, more importantly, off-the-shelf open-source options fail to deliver vectors that are accurate enough for flow estimation while processing high-resolution images at high frequency. We therefore adapted the Depth Inverse Search algorithm from Kroeger et al. [2016] to run entirely on the GPU. The extra speedup enabled us to tune the algorithm so as to obtain measurements that are accurate enough for our purposes. For tuning, we also developed a synthetic image generator that mimics our optical setup and seeding conditions. We describe these developments in detail, and their relevance for the fluid-control community, in [Banelli et al., 2025, Terpin et al., 2025]. Concretely, we mark the region of interest in the wake of the cylinder using AprilTags and leverage them for automatic camera calibration. Full-resolution frames are cropped to a ~ 1 -megapixel window covering this region, resized to 512×512 , and then processed to yield a 512×512 flow estimate. Once the flow field has been estimated, we can linearly downsample it to as few as 16×16 grid points without appreciable loss of salient information (instead, inference on lower-resolution images substantially degrades the estimate).

This is practically interesting, since 16×16 flow estimates are higher dimensional compared to typical feedback used in the fluids-control literature, yet very amenable to state-of-the-art RL methods.

E Ablations

In this section we provide several ablations on (i) the observation sets (see Section E.1), (ii) the model size (see Section E.2), (iii) the way we remove the flow feedback (see Section E.3), and (iv) the learning algorithm employed (see Section E.4).

E.1 Ablations on the observation sets

We complement the results in Section 3.1 by varying the set of observations provided to the agent.

Experimental setup. We use the same physical setup, DreamerV3 architecture, and training protocol as in Section 3.1. For each observation configuration, we train agents for 60 minutes (i.e., 60 episodes, 100,800 environment steps), repeating the training run three times for each configuration. As in the main experiments, the reward is the change in drag relative to its value at the beginning of each episode (decrease for drag minimization, increase for drag maximization), and the drag measurement is always provided as an observation. When we train *without flow feedback*, we additionally provide a normalized episode time index $t = \frac{\text{steps in episode}}{\text{horizon length}}$, the commanded rotation rate and the rotation-rate feedback, or all of these. When we train *with flow feedback*, we additionally provide the 16×16 flow-field estimate. Our main comparison is between families of configurations with and without flow feedback. We focus on flow feedback because it is the only exteroceptive signal in Section 2.

Results. For each configuration, we first average the running-average drag variation over the different repetitions, and then group configurations into two families depending on whether flow feedback is present or not. We then compute, at each training time, the mean across configurations, together with the pointwise minimum and maximum, and the first and third quartiles. Figure 6 reports these aggregated statistics. The resulting trends suggest a qualitative difference between the two tasks. In the drag-maximization setting, configurations without flow feedback show little systematic improvement, whereas configurations with flow feedback more consistently reach higher performance. In contrast, for drag minimization, both families are able to learn high-performing policies, and training without flow feedback appears comparatively easy in this case, although the corresponding configurations exhibit somewhat larger variability. We observe that reported curves differ from the learning curves in Section 3.1, where we show a *single* representative configuration and depict variability across training repetitions of that configuration. In Figure 6, by contrast, we report expected performance and its variability across configurations with and without flow feedback. In particular, when only drag is observed and flow feedback is removed, state aliasing effects can degrade learning performance even in the comparatively easier drag-minimization setting, and these weaker configurations contribute to the aggregate statistics, leading to an apparent decrease in performance even for the drag-minimization task. Nonetheless, the striking contrast remains, and these ablations are consistent with the conclusions of Section 3.1. In our experiments, rich exteroceptive feedback from the flow field is particularly helpful for efficiently finding strong policies in the drag-maximization task, while its role in drag minimization is less pronounced and is mainly reflected in reduced variability across configurations. We note that our coverage of configuration choices is not exhaustive, but these results align with our central claim that feedback during training can

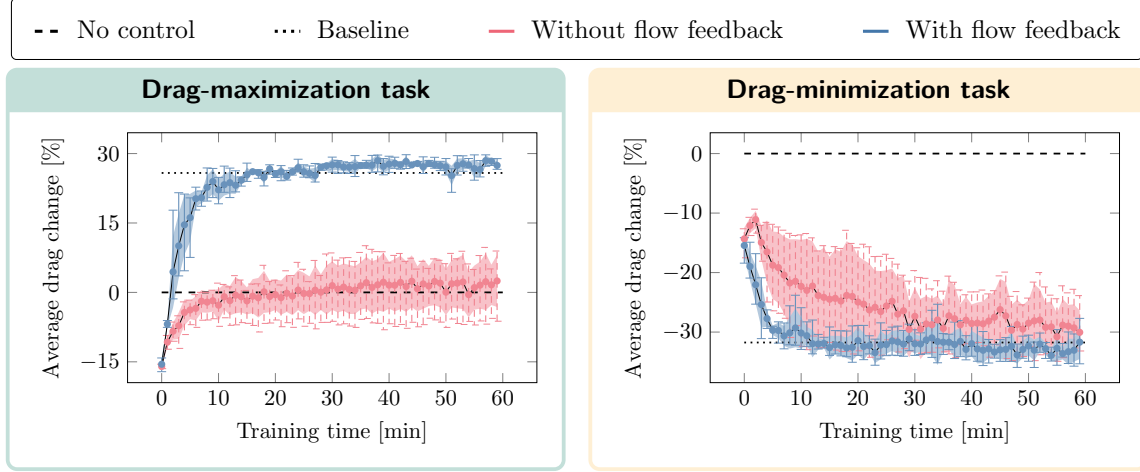


Figure 6: Running-average drag variation (% with respect to no control) over training time for the cylinder drag-maximization (left) and drag-minimization (right) tasks, aggregated over different observation sets. Blue curves correspond to configurations without flow feedback and red curves to configurations with flow feedback. Solid lines show the mean across repetitions and configurations, shaded bands indicate the interquartile range (Q1–Q3), and envelopes denote min–max.

be important for discovering strong policies, even when the resulting control can ultimately be executed with substantially reduced sensory requirements.

E.2 Ablations on the model size

In this section, we study the effect of the model size of DreamerV3 on the learning performance.

Experimental setup. We train the DreamerV3 model with 1 million parameters three times on the drag-maximization task, using as observations the drag, the commanded rotation rate, and its feedback from the motor. We compare it to the 25-million-parameter model in Section 3.1.

Results. We summarize the results in Figure 7, which suggests that the model size does not affect the outcome of the learning process and a larger network is generally better, as suggested by Hafner et al. [2025]. Therefore, the learning failure cannot be attributed to the choice of model size.

E.3 Ablations on how to remove the flow feedback

In this section, we investigate two different approaches for removing the flow feedback for the DreamerV3 model with 25 million parameters.

Experimental setup. We train the DreamerV3 model three times on the drag-maximization task, providing as input a constant, zeroed flow-feedback signal in addition to the drag measurements, the commanded rotation rate, and the rotation-rate feedback. We compare it to the model in Section 3.1, in which the vision branch used for the flow feedback is simply omitted.

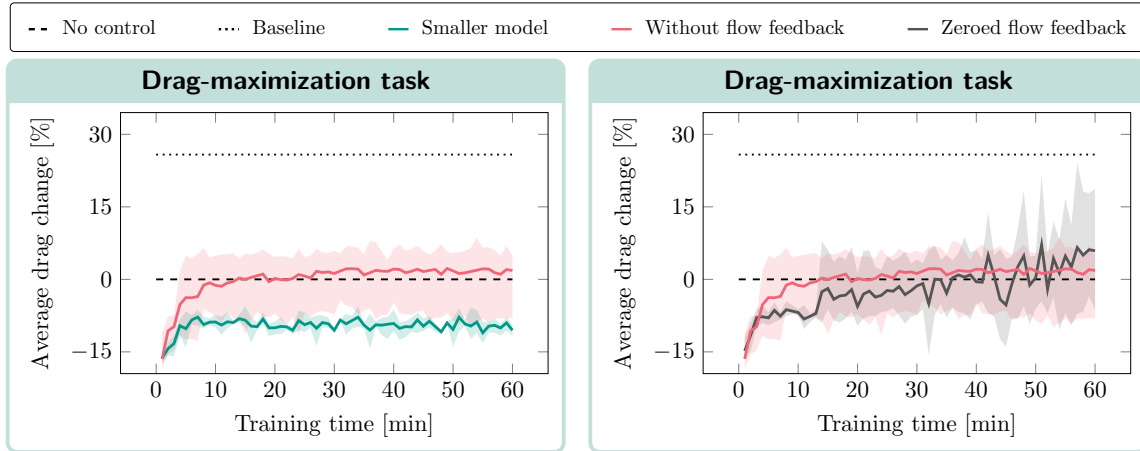


Figure 7: Running-average drag variation (%) with respect to no control) over training time (min) for DreamerV3 in the drag-maximization task. The solid lines show the mean performance of the model across repetitions, whereas the shaded areas show the variability in performance (min-max). The smaller model has 1 million parameters, and the others have 25 million parameters. The model “Without flow feedback” is the same as in Section 3.1. We refer to the model as “Zeroed flow feedback” when a constant, zeroed, flow feedback is additionally provided as input.

Results. We summarize the results in Figure 7, which suggests that the two approaches result in similar performance. In one repetition, the model with zeroed flow feedback seems to perform slightly better in a few rollouts, but overall these results are consistent with the evidence provided in Section 3.1. Thus, in the rest of the paper we use the simpler and more intuitive omission (rather than zeroing) of the flow observation whenever the flow feedback is not provided to the agent.

E.4 Ablations on the learning algorithm

To verify that other state-of-the-art model-free on-policy and off-policy algorithms perform similarly or worse than the DreamerV3 algorithm, we perform an ablation study on the learning algorithm.

Experimental setup. We consider the model-free on-policy PPO algorithm [Schulman et al., 2017] with both a feedforward and a recurrent (–R) network, and the model-free off-policy SAC algorithm [Haarnoja et al., 2018]. We use the stable implementation from Raffin et al. [2021] and, besides the discount factor (which we set to $\gamma = 0.999$ to take into account the horizon length of the task), we use the default hyperparameters. Given the learning speeds observed in Section 3, we provide a budget of 30 minutes. We also provide the agent with the temporal progress observation in all cases additionally to the observations in Section 3, since not all the implementations have recurrent networks.

Results. The resulting learning curves for the drag maximization task are reported in Figure 8. In all cases, the algorithms are unable to solve the task (even when the best-performing one in the first 30 minutes is given ten hours of training). In general, DreamerV3 is less susceptible to hyperparameter tuning and more sample efficient than PPO and SAC, as reported by Hafner et al. [2025]. In fact, the

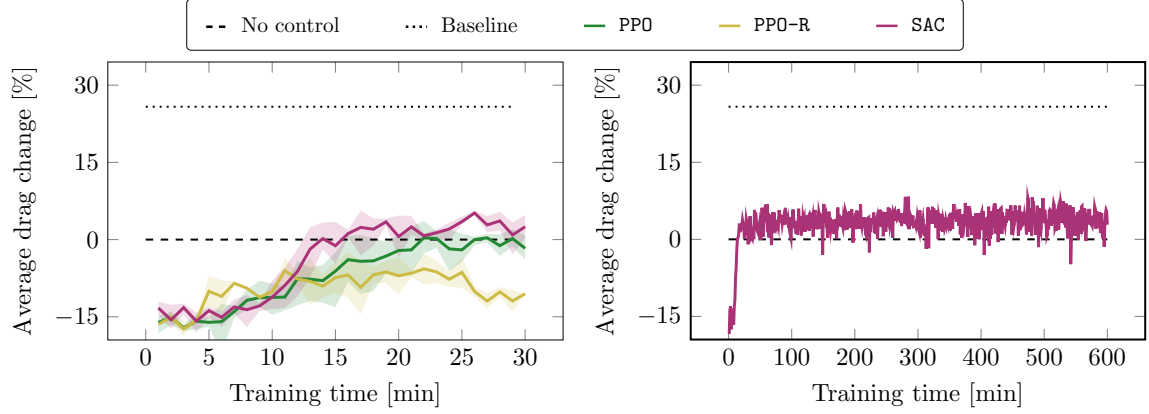


Figure 8: Running-average drag variation (% with respect to no control) over training time (min) for PP0, PP0-R and SAC without flow feedback in the drag-maximization task. The solid lines show the mean performance of the model across repetitions, whereas the shaded areas show the variability in performance (min-max).

experiments in Section 3 show that DreamerV3 learns a high-performance policy within minutes when provided with flow feedback, and longer training budgets are thus not necessary.